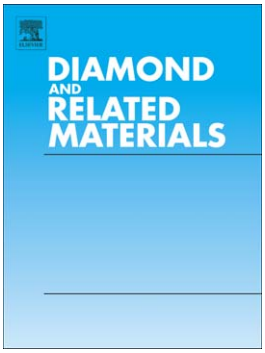

2D inverse periodic opal structures in single crystal diamond with incorporated silicon-vacancy color centers

Bing Dai, Guoyang Shu, Victor Ralchenko, Andrey Bolshakov, Dmitry Sovyk, Andrey Khomich, Vladimir Shershulin, Kang Liu, Jiwen Zhao, Ge Gao, Lei Yang, Pei Lei, Jiaqi Zhu, Jiecai Han

PII: S0925-9635(16)30279-5
DOI: doi:10.1016/j.diamond.2016.09.022
Reference: DIAMAT 6716

To appear in: *Diamond & Related Materials*

Received date: 30 June 2016
Revised date: 23 September 2016
Accepted date: 25 September 2016

Please cite this article as: Bing Dai, Guoyang Shu, Victor Ralchenko, Andrey Bolshakov, Dmitry Sovyk, Andrey Khomich, Vladimir Shershulin, Kang Liu, Jiwen Zhao, Ge Gao, Lei Yang, Pei Lei, Jiaqi Zhu, Jiecai Han, 2D inverse periodic opal structures in single crystal diamond with incorporated silicon-vacancy color centers, *Diamond & Related Materials* (2016), doi:10.1016/j.diamond.2016.09.022

2D inverse periodic opal structures in single crystal diamond with incorporated silicon-vacancy color centers

Bing Dai[a#], Guoyang Shu[a#], Victor Ralchenko[a,b,c], Andrey Bolshakov[b,c], Dmitry Sovyk[b,c], Andrey Khomich[b,d], Vladimir Shershulin[b], Kang Liu[a], Jiwen Zhao[a], Ge Gao[a], Lei Yang[a], Pei Lei[a], Jiaqi Zhu[a]*, Jiecai Han[a]

[a]*Center for Composite Materials and Structures, Harbin Institute of Technology, Harbin 150080, P. R. China*

[b]*General Physics Institute RAS, Vavilov str. 38, Moscow 119991, Russia*

[c]*National Research Nuclear University MEPhI, Moscow 115409, Russia*

[d]*Institute of Radio Engineering and Electronics RAS, Fryazino 141190, Russia*

*Corresponding author: Jiaqi Zhu (zhujq@hit.edu.cn)

# These two authors contributes equally to this work.

Abstract

Well-ordered opal-diamond composite and inverted opal structure in single crystal (SC) diamond have been prepared by microwave plasma CVD. The process is based on epitaxial diamond growth through a monolayer of densely packed SiO_2 spheres placed on a (100) HPHT diamond substrate. Finally, the opal monolayer with ≈ 600 nm sphere diameter was completely embedded in SC CVD diamond forming a new type of ordered diamond composite. In addition, the inverse opal structures (air cavities in diamond) were produced by SiO_2 etching. The XRD analysis confirmed the single crystal nature of the deposit. The photoluminescence spectrum exhibits a strong peak at 738 nm wavelength of silicon-vacancy defect in diamond, indicating Si doping during the CVD process. The optical properties of the diamond structures were evaluated also with Raman spectroscopy and optical reflection spectrometry. The developed epitaxy-through-mask approach is considered as a potential strategy to fabricate multilayered (3D) SC diamond photonic crystals.

Keywords: single crystal diamond, MPCVD, opal structure, silicon-vacancy center, photonic crystal

1. Introduction

Diamond, with its wide optically transparent window, coupled with excellent thermal and mechanical properties, and highly stable color centers, attracts an increasing attention for use in multispectral optical applications, including windows and components for high power IR lasers

[1], compact Raman lasers [2,3], quantum information technologies [4], optical biomarkers [5], UV detectors [6], optical components of complex shapes like lenses [7], waveguides [8] and diffractive optical elements [9]. Due to relatively high refractive index *n*=2.4, diamond is also of interest for building photonic crystals (PhCs) operated from visible to IR region. The PhCs are media with dielectric constant varied periodically with the period of optical wavelength scale, possessing unusual optical properties due to existence of partial or complete photonic band gap (PBG) [10], which is usually explored to suppress, slow, confine or guide electromagnetic waves in certain lattice directions. Therefore, the PhCs are regarded to be important for realization of various optoelectronic and quantum-optical devices, such as low-threshold lasers [11]. Currently, colloidal-assembled opal structures, which consist of SiO_2 spheres typically of a few hundreds of nanometers diameter packed in a face-centered cubic lattice, are widely used as PhC medium, and as the template to reproduce other forms (which also are PhCs), like inverse opals obtained by etching the primary opal matrix, or composites by filling the pores with appropriate optical material [12,13]. To obtain the full PBG in inverse opal (IO) structure, one kind of filling materials with refractive index of 2.8 or larger is strongly required [14]. One of the interesting materials for IO is regarded to be single crystalline diamond with its relatively refractive index of 2.4. The slight difference of refractive index makes a pseudo-PBG other than a pure PBG. Moreover, besides of the excellent physical and chemical properties, diamond has a better refractive index contrast compared to common transparent in the visible materials, like oxides (TiO_2[15] or $BiFeO_3$[16] being a few exclusions), making it a preferential candidate for PhC engineering.

PhCs based on porous inverse opal structures and composites based on oxides, polymers, and semiconductors have been well studied during several decades [13]. However, there are only few works on PhCs made of high refractive index materials, such as diamond. The diamond PhC fabrication process could be achieved based on template-mediated (also known nano-casting) technique using bulk or thin film porous opals. Atypical IO structure with period in the range of 300~ 600 nm can be obtained by seeding the pores with nano-diamond particles, accompanied with depositing CVD diamond and etching away the template [12, 18-20]. However, the used replica approach can produce principally nanocrystalline structures only, as the diamond nucleation and growth proceeds epitaxially on randomly oriented nano-seeds. The nanocrystalline diamond possesses strongly enhanced optical absorption and low thermal conductivity [21], thus loosing in a part the potential advantageous of diamond for the optical applications. In this manuscript, we fabricated for the first time and studied single crystal (SC) diamond with buried monolayer SiO_2 opal structure and IO structure, using a new approach of diamond epitaxy on SC diamond substrate by chemical vapor deposition through a SiO_2 opal

monolayer serving as a mask. We show that the diamond can growth through narrow pores with several tens of nanometers between SiO_2 spheres, remaining single crystal structure. This diamond opal structure exhibits attracting optical properties which makes it be a potential candidate for photonic crystals.

2. Experimental

The developed approach is shown schematically in Fig. 1. First, an ordered opal monolayer was deposited onto the surface of (100) oriented type Ib HPHT diamond substrate ($3\times3\times1$ mm^3) by Langmuir-Blodgett (LB) method. At the next step, epitaxial diamond film was grown through the voids between the SiO_2 spheres, using a microwave plasma chemical vapor deposition (MPCVD) in CH_4/H_2 mixtures. Finally, the opal layer was completely buried in the diamond, and then the SiO_2 spheres were removed by HF acid etching to produce the diamond inverse opal structure.

Fig.1. Schematics of single crystal diamond inverse opal preparation.

The opal monolayer (ML) was formed of SiO_2 spheres with average diameter $d = 615\pm$ 20 nm using a LB trough (Biolin KSV NIMA). The HPHT diamond substrate, oxygen-terminated by heating in oven in air (500°C, 30 min) to get hydrophilic surface, was vertically immersed into the SiO_2 sphere suspension in ultra-pure deionized water. When the spheres assembled into regular array on the water surface by two moving barriers in the LB trough, the substrate was lift up under constant speed 1.5 mm/min, resulting in transfer of the ordered monolayer silica LB film onto HPHT diamond surface.

The diamond film was deposited onto the monolayer opal structure with a MPCVD system (PLASSYS SSDR 150, 2.45 GHz) using the following process parameters: gas mixture of 4%CH_4 diluted in H_2, pressure of 110 mbar, microwave power of 3300 W, growth rate at ≈1 μm/h. The substrate temperature of 700°C was maintained in order to reduce the etching of silica spheres under hydrogen plasma environment. Another growth experiment was performed with a MPCVD system (ARDIS-100, 2.45 GHz) using slightly different process parameters: 8% CH_4 diluted in H_2, pressure of 53 mbar, microwave power of 2200 W, growth rate of ≈1.2 μm/h. Those conditions provided the same low substrate temperature (≈700°C). Very similar diamond layers in terms of surface morphology, Raman and photoluminescence were obtained with these two MPCVD systems to increase the number of samples available for analysis.

The growth time was controlled to obtain several particular diamond opal composite systems with different thicknesses of the diamond film. The sidewalls of the fully covered composite sample were polished in order to open the SiO_2 spheres and then to remove them by HF acid etching to form regular cavities within SC diamond. Further, the samples were heated at 580°C in air to remove the non-diamond carbon contamination on the cavities surface, if any, while the diamond component was retained.

The morphology of samples was studied by scanning electron microscopy (SEM) (FEI Quanta 2000). An atomic force microscope Ntegra Spectra, (NT-MDT) was also engaged to the surface topography measuring. The surface scanning was carried out in semi-contact mode using a silicon HA-NC probe (NT-MDT), with tip radius of curvature of 10 nm.

The single crystal structure of the deposited CVD diamond layers was checked with XRD (Philips X'pert MRD). Raman and photoluminescence (PL) spectra, excited at 473 nm, were measured with a LabRam HR800 (Horiba Jobin-Yvon) spectrometer with the spectral resolution of 1.0 cm^{-1} and spatial resolution of ~1 μm. The laser beam was focused on the sample surface, and the light from the sample has been collected in back-scattering geometry with the microscope objective (Olympus, magnification ×100, numerical aperture NA = 0.90). Optical reflection spectra were measured with an "HR2000+CG" spectrometer (Ocean Optics) in the visible-near IR region (0.3~1.1 μm) at normal incidence, the probed spot size was less than 1 mm.

3. Results

The as-deposited SiO_2 spheres exhibited a well ordered 2D hexagonal lattice structure as demonstrated in Fig. 2a. The diamond deposition resulted in epitaxial growth up from bottom due to reaction species penetrating through the pores to the HPHT diamond substrate surface to maintain the epitaxy. The CVD diamond layer with the height of a half sphere diameter (≈300 nm) was formed for 15 min growth with the PLASSYS MPCVD machine, without a noticeable disturbance of the opal lattice (Fig. 2b). The following growth for total time of 60 min resulted in the diamond film thickness exceeding the opal layer height, the SiO_2 spheres being surrounded by regular diamond ridges with flat (100) tops (Fig. 2c). The pits yet are not closed, this indicating the incomplete overgrowth. However, the pits almost disappear due to lateral diamond growth after continuation of growth process up to 90 min. Smooth surface forms with only rear pits survived (Fig. 2d). Similar completely overgrown samples were produced with ARDIS-100 MPCVD system, but for shorter deposition time (≈70 min), according to the difference in the diamond growth rate.

Fig. 2. SEM images of the opal monolayer at different stages of the diamond deposition process: (a) as-deposited opal layer; (b) half sphere diameter overgrowth for 15 min; (c) complete overgrowth (60 min); (d) further diamond growth to obtain a smooth surface (90 min). Tilt angle is 0° (a) and 45° (b-d).

The AFM image of a selected pit with dimensions ≈1 × 1.5 μm^2, on a 5×5μm^2 area, and its linear profile in cross section, as taken on completely buried opal ML, are shown in Fig. 3. Some of sidewalls look quite smooth. Also, the SEM images at higher magnifications (see one of them in Fig. 8) confirm that the pit sidewalls are generally as smooth as the plane surface. Fine surface features, seen outside of the pit, contribute to global roughness. As a typical value, the roughness R_a = 9.3 nm was measured on 15×15 μm^2 area free of the pits. The pit depth of 400 nm and ≈40° slope are found from cross section profile of the pit (Fig. 3b).

Fig. 3. AFM image of a selected pit with dimensions ≈1 ×1.5 μm^2: 3D image (a) and the profile in cross section in direction shown by arrows (b).

In addition, we measured surface roughness *R*a for the same sample, but on much larger area of 356×267 μm^2 (it contained a number of the pits), using the optical profilometer. The low value *R*a = 4.8 nm was obtained, arguing in favor of single crystal structure of the epitaxial film. No grain boundaries, typical for polycrystalline films, were revealed. The roughness determined by this instrument is less than the AFM derived data since the lateral resolution of the optical profilometer is limited by a light wavelength.

The (400) XRD polar diagram (not shown here) confirmed the single crystalline nature of the deposited diamond. In view of small thickness, of the order of 1 μm, of the CVD layer the XRD signal could be masked by a stronger contribution from the HPHT substrate. For this reason a grazing incidence XRD (Cu anode, incidence angle 1°, resolution 0.01°, scanning rate 4°/min) was also performed for 2θ diffraction angles in the range of 0 – 100° to reduce the information depth (Fig. 4). No diffraction peaks that could be attributed to polycrystalline structure have been revealed.

Fig. 4. Grazing incidence XRD of the micro-level CVD layer, shows no diamond 2θ diffraction peaks through all angles, which indicate that the structure is not polycrystalline.

The Raman spectrum for the completely overgrown sample revealed a sharp diamond peak at 1332.4 cm^{-1} with small width (FWHM) of 2.6 cm^{-1}, characteristic for high quality single crystalline diamond, as displayed in Fig. 5a (top spectrum). The sample before etching the SiO_2 balls, contains a small amount of non-diamond carbon as evidenced from a broad band in the range of 1440 to 1630 cm^{-1}, composed of trans-polyacetylene (t-PA) band (1450 cm^{-1}) and G-band of sp^2 graphitic phase at 1550~1620 cm^{-1} wavenumbers [22]. The band at 504.4 nm, also seen in the spectrum, is the photoluminescence line from N-V-N center in the HPHT substrate. This was confirmed by taking Raman spectrum from the rear side of the substrate and observation of even stronger the 504.4 nm PL line. The a-C inclusions may form at SiO_2/diamond interface within narrow gaps, especially in the vicinity of the SiO_2 balls contact with the substrate, where H and CH_x radicals are subjected to recombination on surfaces. The reduction in atomic hydrogen concentration withdraws the local gas composition beyond the diamond-forming domain and promotes graphite-like carbon deposition. Indeed, this sp^2 carbon contamination was removed by HF acid treatment in course of IO preparation followed by annealing in air (580°C, 30 min), as confirmed by the reduction in intensity of non-diamond bands in the Raman spectrum (see bottom spectrum in Fig. 5a). The quality factor $Q_1 = I_d/I_{nd}$ for the film, defined as the ratio of diamond Raman peak integral intensity I_d (area under peak) to the intensity of all non-diamond bands I_{nd} (t-PA plus G-band, but without PL band from N-V-N) increases by ten times, from Q = 0.6 to Q = 6.0 after the etching and annealing in air. Another version of the quality factor $Q_2 = I_d/I_G$ defined as the ratio of diamond Raman peak integral intensity to the intensity of G-band, improves even stronger, from 1.0 to 12.2. Moreover, some narrowing of the diamond peak to 2.4 cm^{-1} (FWHM) is observed after the etching due to removal of nanocrystalline diamond inclusions on spherical cavity surface. The resulting inverse opal structure as seen in cross section, is displayed in Fig. 6.

Fig. 5. Raman spectra for diamond-opal composite grown for 90 min (top) and inverse opal produced by etching of the composite in HF, followed by oxidation in air (bottom spectrum) (a); PL spectra for diamond-opal composite (b). The PL peaks at 575 nm and 738 nm belong to NV^0 and SiV color centers, respectively.

Fig.6. SEM image of polished cross-section after the sample was treated by HF to etch away the SiO_2 spheres in order to form a monolayer of cavities.

The photoluminescence spectrum exhibits a strong PL peak at 738 nm of silicon-vacancy defect in diamond (Fig. 5b). Also seen in the spectrum is a weak band at 575 nm of neutral

nitrogen-vacancy (NV^0) color center, while the peak at 637 nm from negatively charged NV^- center hardly can be identified. The nitrogen presence in the growth environment was due to residual impurity in source gas (methane). The SiV center was formed as a result of SiO_2 spheres etching by atomic hydrogen of the plasma at early stage of growth, formation of gaseous SiH_x radicals with successive Si atom incorporation in the growing diamond layer. This Si doping effect was observed earlier for nanocrystalline inverted opals grown by MPCVD [18]. While the Si doping of SC diamond to obtain SiV centers is a subject of many ongoing researches [23,24], the incorporation of SiV centers into SC diamond-opal composite and inverted 2D SC diamond opal structure is realized, to our knowledge, for the first time.

Further information on the optical properties of the samples was obtained from reflectivity spectra. The illuminated side was always the CVD layer. Fig. 7 shows the reflection spectra for (i) bare HPHT substrate, (ii) the substrate with ML opal, (iii) the diamond film with buried ML opal, and (iv) the same sample after etching SiO_2 spheres. The bare HPHT Ib type diamond displays a dip at wavelengths below 550 nm due to strong optical absorption by nitrogen impurity [25], so the contribution of reflection from the rear surface of the substrate is reduced. This dip is present to some extent in reflection spectra of all coated samples. The spectrum for ML opal before diamond growth displays several oscillations with maxima at 472, 657, 753 and 1068 nm (the latter peak is not shown here).

For opal monolayer the reflection peak (or transmission dip) takes place at wavelengths $\lambda \approx d$, where d is sphere diameter [26,27], that can be associated with optical eigen-modes of 2D PhC [26]. Therefore we refer the observed 657 nm peak to that resonance. Other maxima are assumed to correspond to Fabry-Perot (F-P) oscillations in the opal layer, which have a good contrast due to high refraction index of the substrate. The observed frequent fringes in the reflection spectra for completely overgrown SiO_2 spheres and for inverted diamond opal produced by etching the SiO_2, are attributed to F-P modes in thin CVD diamond layer (cap) on the top of the spheres. The slow modulation of the reflection occurs due to superposition of F-P oscillations in the cap and in buried opal (or in *IO* layer). The effective thickness h of the cap above the spheres (or cavities) was estimated from wavelengths of neighbor maxima in the reflectance spectra $\lambda_{max} = 4nh/(2m - 1)$, where $n = 2.4$ for diamond and m is an integer. The value of $h \approx 700$ nm was found to be in a reasonable agreement with the cap thickness of ≈800 nm assessed from SEM image of film cross section.

Fig. 7. Reflection spectra for (from top to bottom): opal layer completely overgrown by diamond; the same sample after etching SiO_2 spheres; HPHT diamond substrate, and SiO_2 opal monolayer on diamond substrate. The pictograms on the right side assist to sample identification.

Effective refractive index n_{eff} of inverted opal is determined as $n_{eff} = (\varepsilon_{eff})^{1/2}$, where $\varepsilon_{eff} = \varepsilon_v f + \varepsilon_0(1- f)$ is effective dielectric constant, $\varepsilon_0 = 5.76$ is dielectric constant for diamond, f is the volume fraction occupied by voids ($f = 0.74$ for *fcc* lattice), and ε_v is dielectric constant for void material ($\varepsilon_v = 1.0$ for air and $\varepsilon_v = 2.01$ for SiO_2). We found effective refractive index $n_{eff} = 1.50$ and $\varepsilon_{eff} = 2.22$ for *bulk* diamond IO and $n_{eff} = 1.73$ diamond-SiO_2 composite. The Bragg peak is expected to occur at wavelength $\lambda_{max} = 2d\cdot(8/3)^{1/2}\ (\varepsilon_{eff} - \sin 2\theta)^{1/2}$ for the bulk (3D) opaline structures, where θ is light incidence angle ($\theta = 0$ in our experiment). For d =600 nm the Bragg peak lays in the near IR range, at 1469 nm and 1694 nm for IO and diamond-SiO_2 composite, respectively. The SiO_2 sphere diameter reduction in two times to 300 nm is required to match the Bragg peak to SiV zero-phonon line (ZPL) at 738 nm for diamond IO, that technically looks quite possible.

How many opal monolayers packed in a stack are needed to achieve a bulk-like Bragg reflection peak is an interesting question. This minimum number of layers N_c decreases with the value of dielectric contrast $\psi_0 = \varepsilon_{eff}/\varepsilon_v - 1$. For example, for direct SiO_2 opal the contrast is low $\psi_0 = 0.66$ and the critical number of layers is high N_c=13 MLs [28]. For the diamond-air inverse opal, due to high negative contrast $\psi_0 = \varepsilon_{eff}/\varepsilon_0 - 1 = -0.61$, we estimate, according to Ref. [28], the critical thickness (when the stop-band approaches to that for the bulk PhC) of about 3~4 opal monolayers only. The diamond epitaxy through the stack of 3~4 opal MLs looks possible. Our first experiment with a two-ML opal film demonstrated encouraging results as seen in Fig. 8. The diamond growth was interrupted before the complete overgrowth of the opal film in order to display that the structure does contain the two MLs. The first opal layer is already buried in diamond, while the top second layer is only partly covered with the diamond film. Although the ordering of the 2nd layer was not as good as for the bottom layer the result presented in Fig. 8 is regarded as the proof of principle of epitaxial diamond penetration through multilayer opal structures.

Fig. 8. Intermediate stage of overgrowth of a two-layer opal film by diamond film.

4. Conclusions

In summary, we have obtained opal-diamond composite and single crystal diamond monolayer inverse opal, using epitaxial CVD diamond deposition and an opal monolayer as a template. The produced nanostructure is doped with Si to form the SiV centers as confirmed by PL spectroscopy. The single crystal nature of the deposited opal structure diamond assumes much lower optical absorption compared to previously reported nanocrystalline diamond inverse opals.

The developed epitaxy-through-mask technique is a potential strategy to pave the way for fabrication of multilayered (3D) SC diamond PhCs. The developed approach would allow to fully exploit the advantageous optical properties of this material, in combination with ability to incorporate color centers like SiV and NV in the bulk PhC for photonic applications.

Acknowledgments

This work was financially supported by the Fundamental Research Funds for the Central Universities (HIT.NSRIF.2015040), National Key Laboratory Funds (914C490106150C49001) and International Science & Technology Cooperation Program of China (2015DFR50300). This work was also supported by Center for Advanced Laser & Diffusion Wave Technology of Harbin Institute of Technology. The authors are thankful to Yueye Lu for opal layer deposition. The author Bing Dai and Guoyang Shu contribute equally to this work.

References

[1] A. M. Bennett, E. Anoikin. CVD diamond for high power laser applications. Proc. of SPIE, High-power Laser Materials Processing: Lasers, Beam Delivery, Diagnostics, and Applications II, Vol. 8603 (2013) 860307.

[2] R.J. Williams, J. Nold, M. Strecker, O. Kitzler, A. McKay, T. Schreiber, R.P. Mildren, Efficient Raman frequency conversion of high-power fiber lasers in diamond, Laser Photonics Rev. 9 (2015) 405–411.

[3] V.P. Pashinin, V.G. Ralchenko, A.P. Bolshakov, E.E. Ashkinazi, M.A. Gorbashova, V.Yu. Yurov, V.I. Konov, External-cavity diamond Raman laser performance at 1240 nm and 1485 nm wavelengths with high pulse energy, Laser Phys. Lett. 13 (2016)065001.

[4] I. Aharonovich, E. Neu, Diamond nanophotonics, Adv. Opt. Mater. (2014) 911-928.

[5] E. Neu, C. Arend, E. Gross, F. Guldner, C. Hepp, D. Steinmetz, E. Zscherpel, S. Ghodbane, H. Sternschulte, D. Steinmüller-Nethl, Y. Liang, A. Krueger, C. Becher, Narrowband fluorescent nanodiamonds produced from chemical vapor deposition films, Appl. Phys. Lett. 98 (2011) 243107.

[6] M. Girolami, P. Allegrini, G. Conte, D.M. Trucchi, V.G. Ralchenko, S. Salvatori, Diamond detectors for UV and X-ray source imaging, Electron Device Letters, IEEE, 33 (2012) 224-226.

[7] P. Siyushev, F. Kaiser, V. Jacques, I. Gerhardt, S. Bischof, H. Fedder, J. Dodson, M. Markham, D. Twitchen, F. Jelezko, J. Wrachtrup, Monolithic diamond optics for single photon detection, Appl. Phys. Lett. 97 (2010) 241902.

[8] M. Malmström, M. Karlsson, P. Forsberg, Y. Cai, F. Nikolajeff, F. Laurell, Waveguides in

polycrystalline diamond for mid-IR sensing, Opt. Mat. Express, 6 (2016) 1286-1295.

[9] V.I. Konov, Laser in micro and nanoprocessing of diamond materials. Laser Photonics Rev. 6 (2012) 739-766.

[10] J.D. Joannopoulos, P.R. Villeneuve, S. Fan, Photonic crystals: putting a new twist on light. Nature, 386 (1997) 143-149.

[11] M.N. Shkunov, Z.V Vardeny, M.C. DeLong, R.C. Polson, A.A. Zakhidov, R.H. Baughman, Tunable, gap-state lasing in switchable directions for opal photonic crystals. Adv. Func. Mater. 12 (2002) 21-26.

[12] A.A. Zakhidov, R.H. Baughman, Z. Iqbal, C. Cui, I. Khayrullin, S. Dantas, J. Marti, V.G. Ralchenko, Carbon structures with three-dimensional periodicity at optical wavelengths, Science, 282 (1998) 897-901.

[13] E. Armstrong, C. O'Dwyer, Artificial opal photonic crystals and inverse opal structures–fundamentals and applications from optics to energy storage. J. Mater. Chem. C. 3 (2015) 6109-6143.

[14] K. Busch, S. John, Photonic band gap formation in certain self-organizing systems, Phys. Rev. E, 58 (1998) 3896.

[15] J.S. King, E. Graugnard, C.J. Summers, TiO_2inverse opals fabricated using low temperature atomic layer deposition. Adv. Mater. 17 (2005) 1010-1013.

[16] V.V. Abramova, A. Slesarev, A. Sinitskii, Synthesis of high-quality inverse opals based on magnetic complex oxides: yttrium iron garnet ($Y_3Fe_5O_{12}$) and bismuth ferrite ($BiFeO_3$), J. Mater. Chem. C. 1(2013) 2975-2982.

[17] A.B. Pevtsov, A.V. Medvedev, D.A.Kurdyukov, N.D. Il'Inskaya, V.G. Golubev, V.G. Karpov, Evidence of field-induced nucleation switching in opal: VO_2 composites and VO_2 films, Phys. Rev. B, 85 (2012) 024110.

[18] V.G. Ralchenko, D.N. Sovyk, A.P. Bolshakov, A.A. Homich, I.I. Vlasov, D.A. Kurdyukov, V.G. Golubev, A.A. Zakhidov, Diamond direct and inverse opal matrices produced by chemical vapor deposition, Phys. Solid State, 53 (2011) 1131-1134.

[19] D. A. Kurdyukov, N. A. Feoktistov, A. V. Nashchekin, Yu. M. Zadiranov, A. E. Aleksenskii, A. Ya. Vul', V. G. Golubev. Ordered porous diamond films fabricated by colloidal crystal templating, Nanotechnology, 23 (2012) 015601.

[20] D.N. Sovyk, V.G. Ralchenko, D.A. Kurdyukov, S.A. Grudinkin, V.G. Golubev, A.A. Homich, V.I. Konov, Photonic crystals of diamond spheres with the opal structure, Phys. Solid State, 55 (2013) 1120-1123.

[21] V. Ralchenko, S. Pimenov, V. Konov, A.Khomich, A. Saveliev, A. Popovich, I. Vlasov, E. Zavedeev, A. Bozhko, N. Loubnin, R. Khmelnitskii, Nitrogenated nanocrystalline diamond

films: thermal and optical properties, Diamond Relat. Mater. 16 (2007) 2067-2073.

[22] I.I. Vlasov, E. Goovaerts, V.G. Ralchenko, V.I. Konov, A.V. Khomich, M.V. Kanzyuba. Vibrational properties of nitrogen-doped ultrananocrystalline diamond films grown by microwave plasma CVD, Diamond Relat. Mater. 16 (2007) 2074-2077.

[23] L.J. Rogers, K.D. Jahnke, T. Teraji, L. Marseglia, C. Müller, B. Naydenov, H. Schauffert, C. Kranz, J. Isoya, L.P. McGuinness, F. Jelezko, Multiple intrinsically identical single-photon emitters in the solid state, Nature Comm. 5 (2014) 4739.

[24] A. Bolshakov, V. Ralchenko, V. Sedov, A. Khomich, I. Vlasov, A. Khomich, N. Trofimov, V. Krivobok, S. Nikolaev, R. Khmelnitskii, V. Saraykin, Photoluminescence of SiV centers in single crystal CVD diamond *in situ* doped with Si from silane, Phys. Stat. Sol. A 212 (2015) 2525-2532.

[25] H.B. Dyer, F.A. Raal, L. Du Preez, J.H.N. Loubser, Optical absorption features associated with paramagnetic nitrogen in diamond. Phil. Mag. 11 (1965) 763-774.

[26] S.G. Romanov, M. Bardosova, I.M. Povey, M.E. Pemble, C.S. Torres, Understanding of transmission in the range of high-order photonic bands in thin opal film, Appl. Phys. Lett. 92 (2008) 191106.

[27] I. Maurin, E. Moufarej, A. Laliotis, D. Bloch, Optics of an opal modeled with a stratified effective index and the effect of the interface, JOSA B, 32 (2015) 1761-1772

[28] J.F. Bertone, P. Jiang, K.S. Hwang, D.M. Mittleman, V.L. Colvin, Thickness dependence of the optical properties of ordered silica-air and air-polymer photonic crystals, Phys. Rev. Lett. 83 (1999) 300-303.

Figure captions

Fig.1. Experimental approach of single crystal diamond inverse opal.

Fig. 2. SEM images of the opal monolayer at different stages of the diamond deposition process: (a) as-deposited opal layer; (b) half sphere diameter overgrowth for 15 min; (c) complete overgrowth (60 min); (d) further diamond growth to smooth the surface (90 min).

Fig. 3. AFM image of a selected pit with dimensions ≈1 ×1.5 μm^2: 3D image (a) and the profile in cross section in direction shown by arrows (b).

Fig. 4. Grazing incidence XRD of the micro-level CVD layer, shows no diamond 2θ diffraction peaks through all angles, which indicate that the structure is not polycrystalline.

Fig. 5. Raman and PL spectra for diamond-opal composite grown for 90 min. The PL peaks at 575 nm and 738 nm belong to NV^0 and SiV color centers, respectively.

Fig.6. SEM images of the polished cross-section after the sample was treated by HF to etch away the SiO_2 spheres. Cavities at which the spheres stayed were revealed.

Fig. 7. Reflection spectra (from top to bottom) for opal layer completely overgrown by diamond, and the same sample after etching SiO_2 spheres, HPHT diamond substrate and SiO_2 opal monolayer on diamond substrate. The pictograms on the right side assist to sample identification.
Fig. 8. Intermediate stage of overgrowth of a two-layer opal film by diamond film.

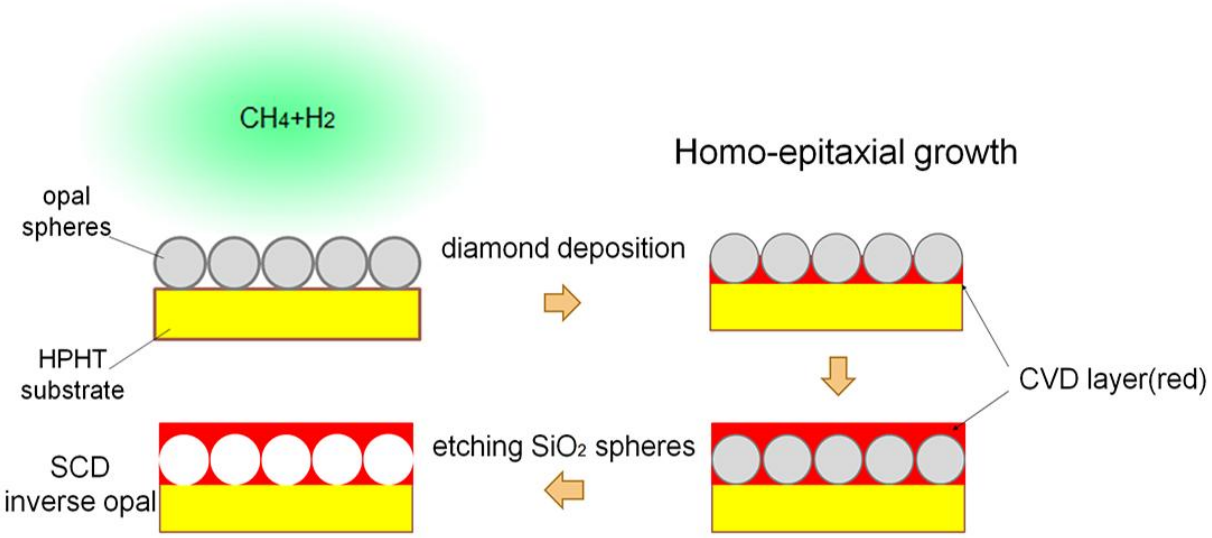

Fig.1. Experimental approach of single crystal diamond inverse opal.

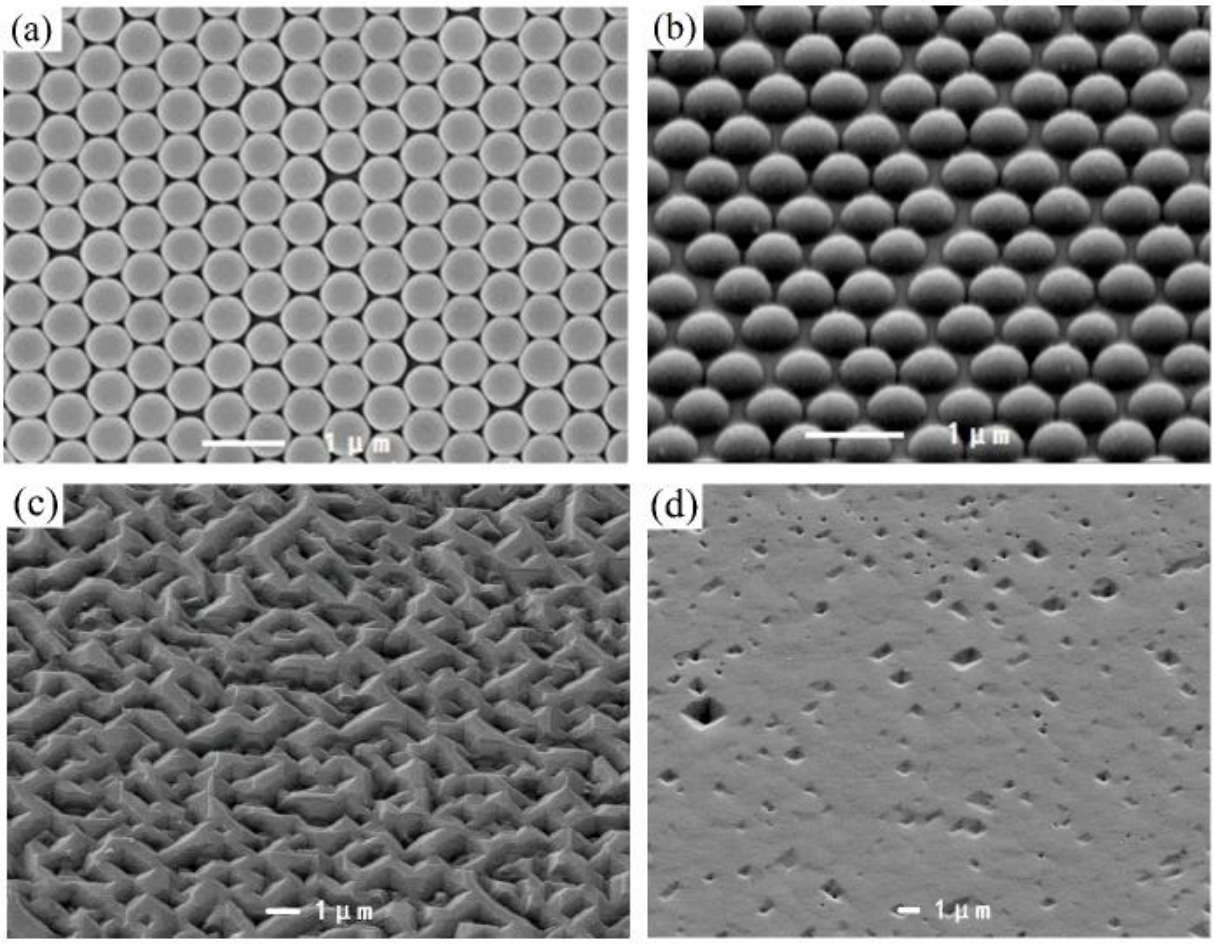

Fig. 2. SEM images of the opal monolayer at different stages of the diamond deposition process: (a) as-deposited opal layer; (b) half sphere diameter overgrowth for 15 min; (c) complete overgrowth (60 min); (d) further diamond growth to smooth the surface (90 min).

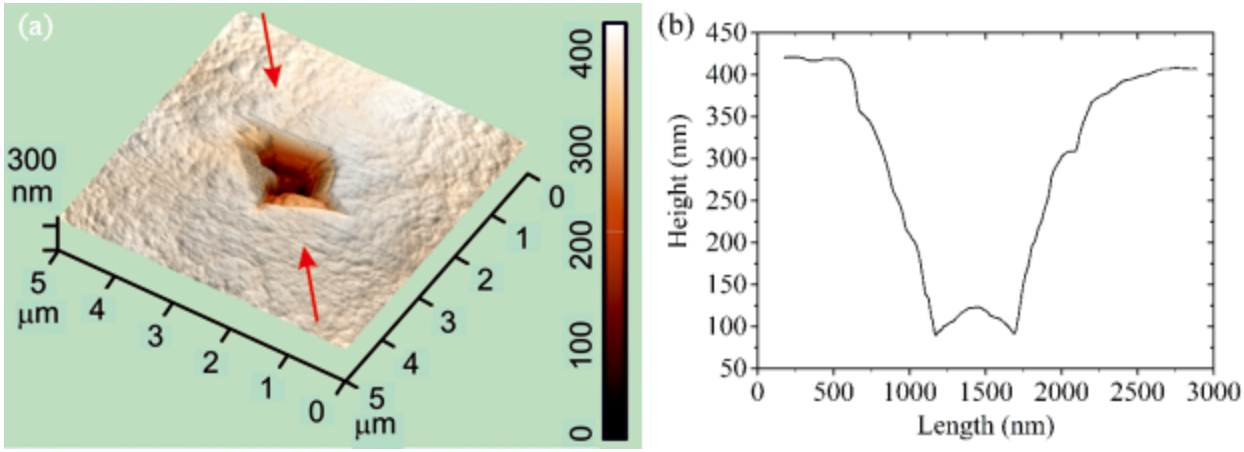

Fig. 3. AFM image of a selected pit with dimensions ≈1 ×1.5 µm^2: 3D image (a) and the profile in cross section in direction shown by arrows (b).

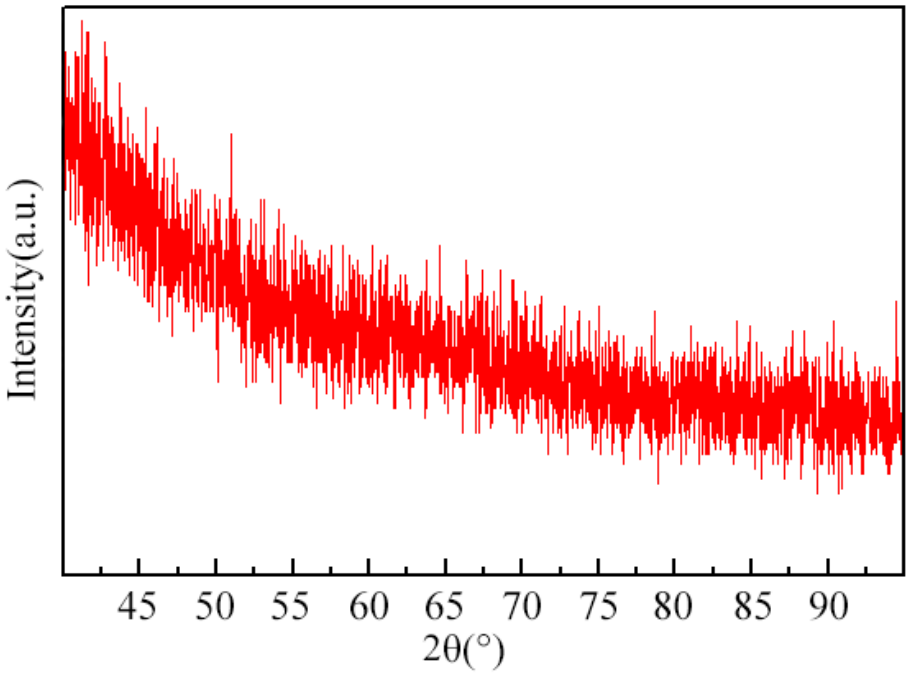

Fig. 4. Grazing incidence XRD of the micro-level CVD layer, shows no diamond 2θ diffraction peaks through all angles, which indicate that the structure is not polycrystalline.

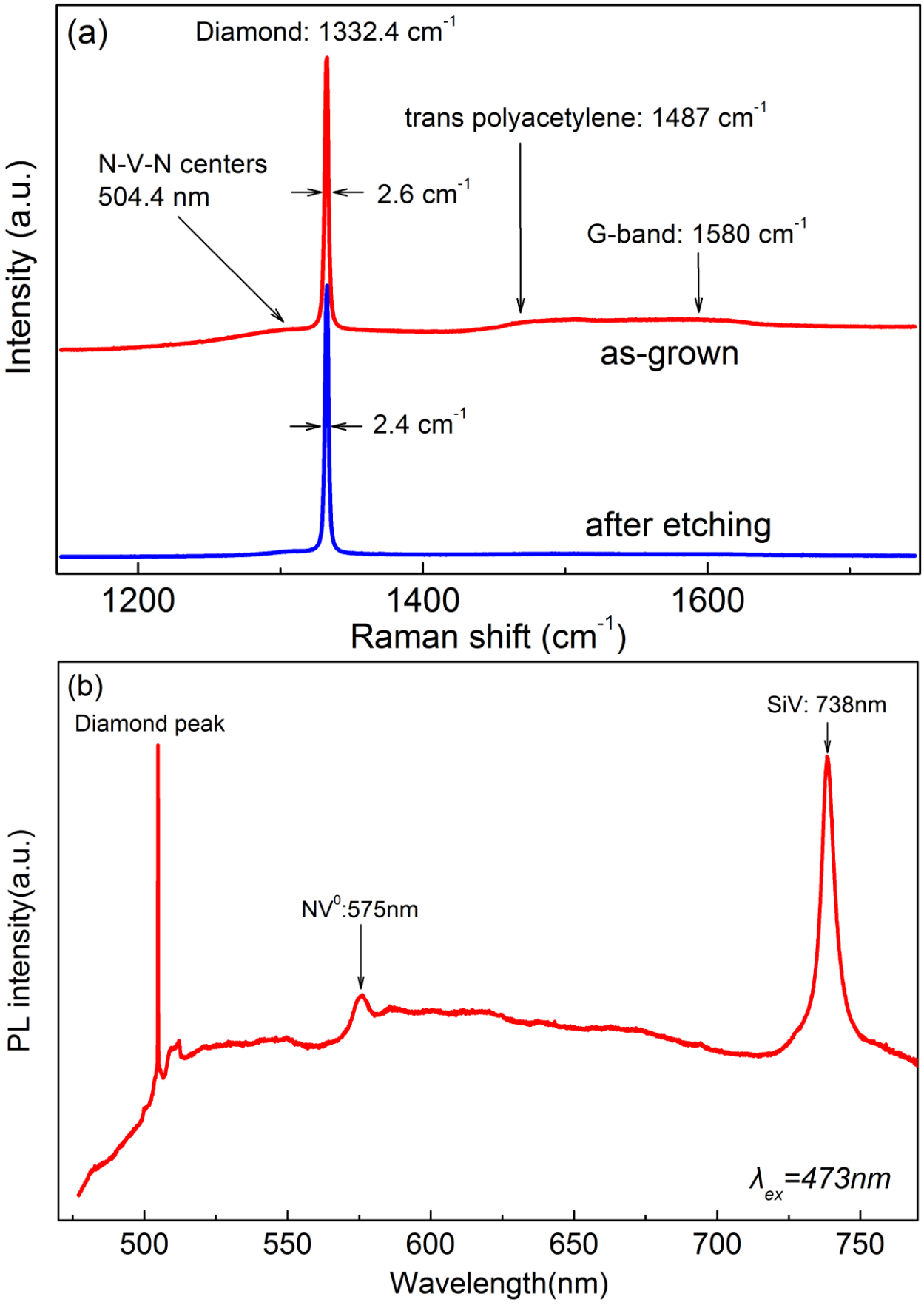

Fig. 5. Raman and PL spectra for diamond-opal composite grown for 90 min. The PL peaks at 575 nm and 738 nm belong to NV^0 and SiV color centers, respectively.

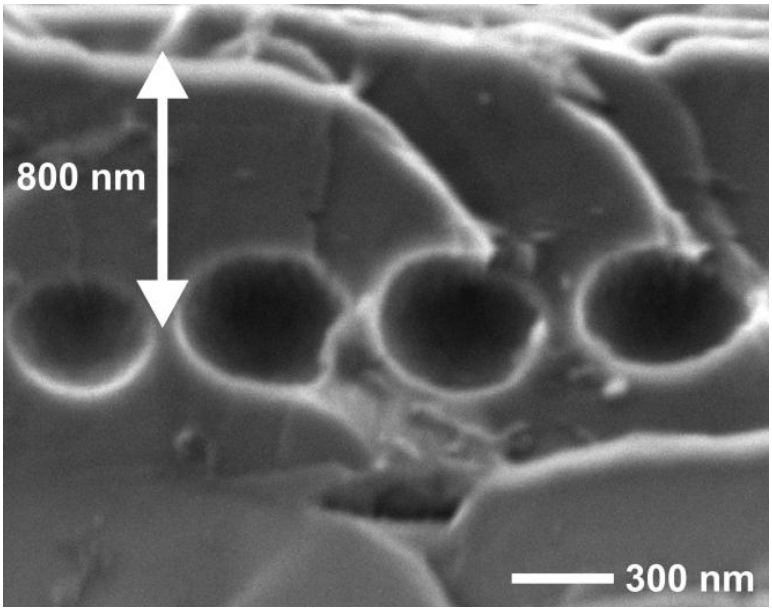

Fig.6. SEM images of the polished cross-section after the sample was treated by HF to etch away the SiO_2 spheres. Cavities at which the spheres stayed were revealed.

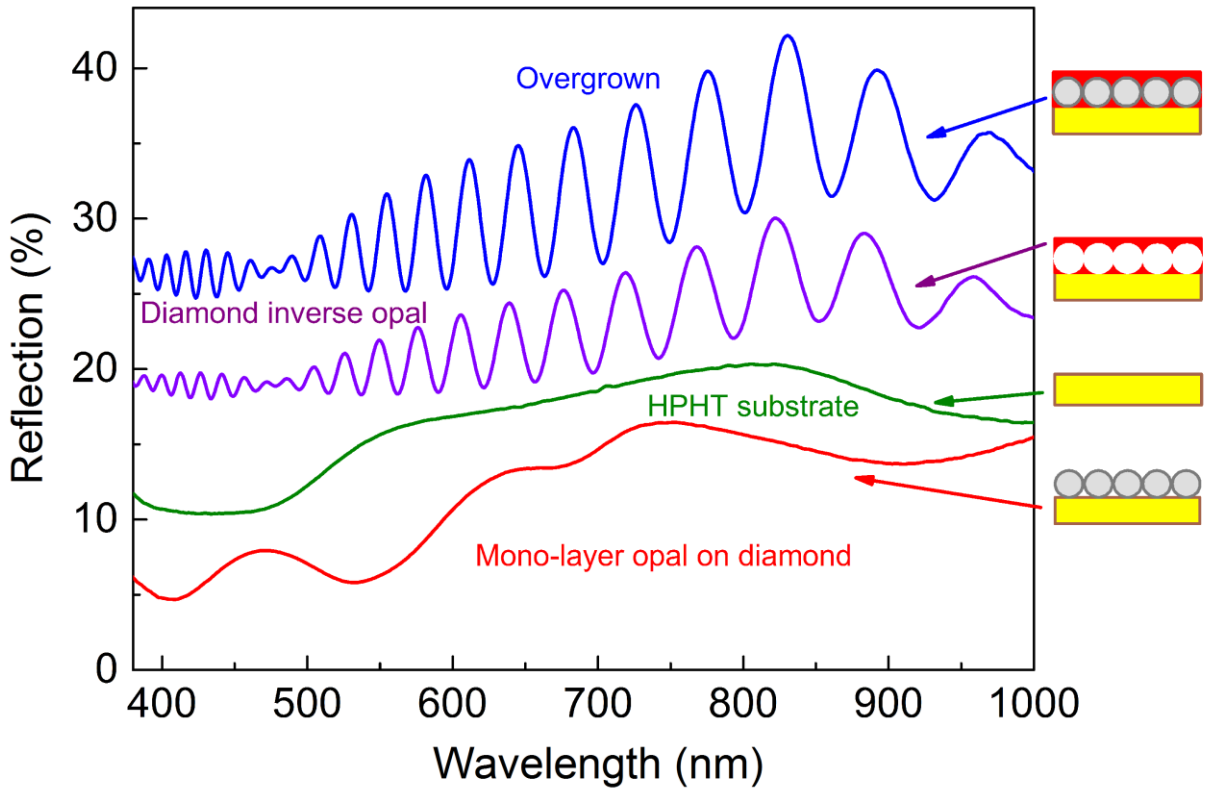

Fig. 7. Reflection spectra (from top to bottom) for opal layer completely overgrown by diamond, and the same sample after etching SiO_2 spheres, HPHT diamond substrate and SiO_2 opal monolayer on diamond substrate. The pictograms on the right side assist to sample identification.

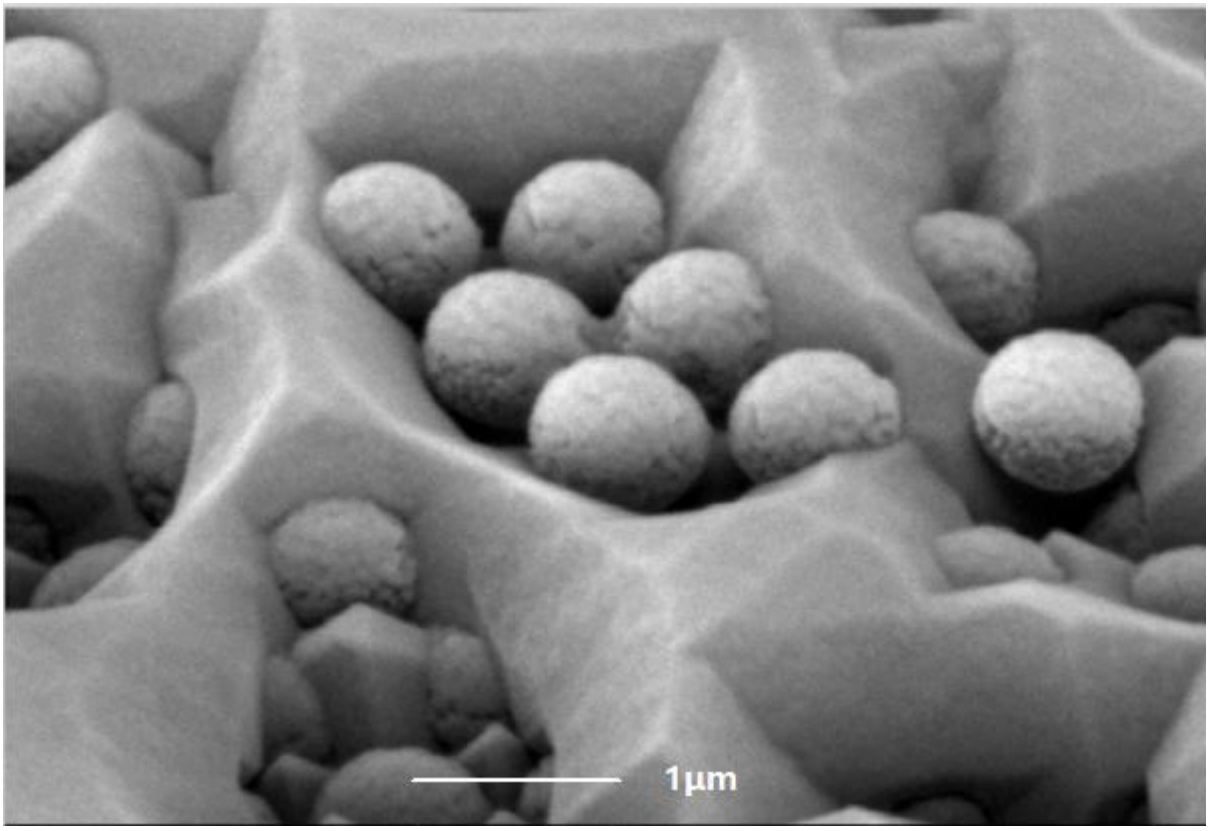

Fig. 8. Intermediate stage of overgrowth of a two-layer opal film by diamond film.

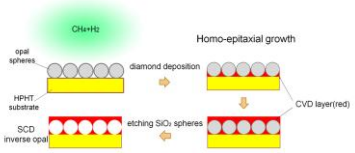

Graphical abstract

Highlight

1. Single crystalline diamond with a buried monolayer opal (SiO_2) nanostructure is grown by MPCVD.

2. Two dimensional inverse diamond opal structure is produced by chemical etching of SiO_2 spheres of the template.

3. The diamond opaline structures are doped with Si and show bright photoluminescence of SiV centers.